Int. J. Heat Mass Transfer. Vol. 35, No. 8, pp. 1935–1945, 1992
Printed in Great Britain

0017–9310/92 $5.00+0.00

Natural convection between concentric spheres

VIJAY K. GARG†
Department of Mechanical Engineering, University of Pittsburgh, Pittsburgh, PA 15261, U.S.A.

(*Received* 13 *February* 1991 *and in final form* 17 *July* 1991)

Abstract—A finite-difference solution for steady natural convective flow in a concentric spherical annulus with isothermal walls has been obtained. The stream function–vorticity formulation of the equations of motion for the unsteady axisymmetric flow is used; interest lying in the final steady solution. Forward differences are used for the time derivatives and second-order central differences for the space derivatives. The alternating direction implicit method is used for solution of the discretization equations. Local one-dimensional grid adaptation is used to resolve the steep gradients in some regions of the flow at large Rayleigh numbers. The break-up into multi-cellular flow is found at high Rayleigh numbers for air and water, and at significantly low Rayleigh numbers for liquid metals. Excellent agreement with previous experimental and numerical data is obtained.

1. INTRODUCTION

BUOYANCY-DRIVEN flows in enclosures are of importance in various applications such as in nuclear reactor design, aircraft cabin insulation, cooling of electronic equipment, and thermal storage systems. In particular, natural convection heat transfer in the annular space between concentric cylinders and spheres has drawn considerable attention. Several numerical and experimental studies of natural convection within a spherical annulus for various values of the Prandtl and Rayleigh numbers are available. Several types of flow patterns inside the concentric spheres have been observed for various gap–radius ratios, Prandtl and Rayleigh numbers. Flow patterns may consist of one cell, the crescent eddy type or kidney-shaped eddy type, or may be multi-cellular for low diameter ratios and high Rayleigh numbers.

Experimental data on natural convection between isothermal concentric spheres, the inner being hotter, have been provided by Bishop *et al.* [1, 2], Scanlan *et al.* [3] and Yin *et al.* [4] for a very wide range of Prandtl and Rayleigh numbers. Temperature distribution within the annulus was measured and Nusselt–Grashof number correlations were presented. Temperature profiles and flow patterns were, however, presented for various temperature differences between the two spheres rather than for various Rayleigh numbers. This makes direct comparison of temperature distribution difficult since the mean temperature for fluid property calculation is often unspecified, making it difficult to estimate the Rayleigh number. Amongst the numerical methods, Mack and Hardee [5] developed a perturbation solution for the steady axisymmetric convection within the isothermal concentric spherical annulus. They carried the solution to terms proportional to the third power of the Rayleigh number, and so could only present results for Rayleigh number, $Ra = 1000$, and Prandtl number, $Pr = 0.7$. In fact, the temperature profiles in their Fig. 3 for $\phi \leqslant 40°$ are in error, thus implying that even at the low Ra of 1000, higher-order terms, neglected in their solution, are essential for accuracy. Brown [6] used explicit finite-difference techniques for numerical integration of the governing equations, and presented results for $Pr = 0.7$. His Nusselt number values are about 10% higher than the experimental values for all diameter ratios except the smallest.

Singh and Chen [7] developed a series solution in terms of Legendre polynomials and Gegenbauer functions for the same problem. They are able to obtain results for Ra up to 9×10^4, though they admit that their results for $Ra = 9 \times 10^4$ and $Pr = 6$ are in error due to premature truncation of the series solution. Moreover, for $Pr = 0.02$, Singh and Chen [7] could not get convergence for $Ra = 400$. We confirm this and present the accurate results for these cases, and for much higher Rayleigh numbers. Caltagirone *et al.* [8] carried out a finite-difference solution of the unsteady equations for natural convection between isothermal concentric spheres in order to get the steady-state solution. However, they found two different numerical solutions for a given set of parameters. Ingham [9] presented numerical results for a diameter ratio of 1.19 but found no multi-cellular flow up to a Rayleigh number, based on the gap width, of 1.7×10^5 for air. Fujii *et al.* [10] used a finite-difference alternating direction implicit method and a successive over-relaxation method but provided results only for very large diameter ratios. Their aim was to find a critical value of the diameter ratio at which heat transfer from the inner sphere is no longer influenced by the presence of the outer sphere.

Singh and Elliott [11] carried out a power series solution for a thermally stratified medium between concentric spheres. The inner sphere was kept either at a constant temperature or constant heat flux, and the outer sphere was maintained at a variable tem-

†Present address: NASA Lewis Research Center, Mail Stop 5-11, Cleveland, OH 44135, U.S.A.

NOMENCLATURE

a_θ, a_Ψ, a_Ω	false transient factors
g	acceleration due to gravity
Gr	Grashof number based on the gap width
k	thermal conductivity of the fluid
k_{eff}	effective thermal conductivity of the spherical annulus
Nu	local Nusselt number
$\overline{Nu}$	average Nusselt number
Pr	Prandtl number of the fluid
r	radial coordinate measured from the center of the spheres
r_i, r_o	radii of inner and outer spheres, respectively
R	dimensionless radial coordinate
Ra	Rayleigh number based on the gap width = $Gr\,Pr$
S	speed of fluid within the annulus ($S^2 = U^2 + V^2$)
t	time
T	temperature of the fluid
T_i, T_o	temperature of the inner and outer spheres, respectively
u	velocity component in the ϕ direction
U	dimensionless velocity component in the ϕ direction
v	radial velocity component
V	dimensionless radial velocity component
X	dimensionless radial coordinate.

Greek symbols

α	thermal diffusivity of the fluid
β	coefficient of volumetric expansion of the fluid
ΔR	mesh size in the radial direction
$\Delta\phi$	mesh size in the ϕ direction
$\Delta\tau$	dimensionless time step
θ	dimensionless temperature
ν	kinematic viscosity of the fluid
τ	dimensionless time
ϕ	latitude angle measured clockwise from the North position
ψ	dimensional stream function
Ψ	dimensionless stream function
ω	dimensional vorticity
Ω	dimensionless vorticity.

Subscripts

b	value at the boundary
b+1	value at one mesh length ΔR away from the boundary
i	value at the inner sphere
o	value at the outer sphere
r	refers to radial direction
ϕ	refers to latitude direction
max	maximum value.

perature for vertical stratification. They presented results for $Pr = 0.7$ and very low Rayleigh numbers. Mojtabi and Caltagirone [12] used a spectral method to obtain results for an infinite Prandtl number, and studied its linear stability. Nelsen *et al.* [13], Nelsen and Douglass [14, 15], and Wright and Douglass [16] analyzed natural convection in a spherical annulus filled with a heat generating fluid, while Gardner *et al.* [17] analyzed its linear stability characteristics for small gap widths (inner to outer sphere radius ratios of 0.9 and 0.95). Burns and Tien [18] used finite-differences and regular perturbations for the study of natural convection in porous media bounded by concentric spheres and horizontal cylinders.

From the above description, it is apparent that accurate numerical solution of the natural convective flow within a concentric spherical annulus at realistically high Rayleigh numbers is not available. Also, break-up into multi-cellular flow has not been predicted though it has been observed experimentally. We, therefore, describe a finite-difference method that is fast, reliable and accurate for any value of the Rayleigh number for the steady axisymmetric natural convection heat transfer of a viscous fluid enclosed between two isothermal concentric spheres, and we find the steady multi-cellular flow at high Grashof numbers for all Prandtl numbers. The equations of motion for the unsteady flow are solved to get the steady-state solution. Local one-dimensional grid adaptation is used to resolve the steep gradients in some regions of the flow at large Rayleigh numbers. This maintains orthogonality of the grid, unlike a two-dimensional grid adaptation, thereby avoiding the need to solve the complex transformed equations for a non-orthogonal coordinate system. The alternating direction implicit method is used for the solution of the algebraic equations. The method can also be applied to other geometries and boundary conditions.

2. ANALYSIS

Consider a constant property, except for density, Newtonian fluid contained within a concentric spherical annulus. Assuming unsteady, axisymmetric, laminar natural convective flow caused by the inner hot and outer cold isothermal spheres, and using the Boussinesq approximation and spherical coordinates, the dimensionless energy and Navier–Stokes equations in the stream function–vorticity form are

$$Pr\frac{\partial\theta}{\partial\tau} + Pr\,Gr^{1/2}\left(V\frac{\partial\theta}{\partial R} + \frac{U}{X}\frac{\partial\theta}{\partial\phi}\right) = \nabla^2\theta, \qquad (1)$$

$$D^2\Psi + X\Omega \sin\phi = 0, \tag{2}$$

$$\frac{\partial\Omega}{\partial\tau} + Gr^{1/2}\left[V\frac{\partial\Omega}{\partial R} + \frac{U}{X}\frac{\partial\Omega}{\partial\phi} - \frac{\Omega}{X}(V + U\cot\phi)\right]$$
$$= -Gr^{1/2}\left(\sin\phi\frac{\partial\theta}{\partial R} + \frac{\cos\phi}{X}\frac{\partial\theta}{\partial\phi}\right) + \nabla^2\Omega - \frac{\Omega}{X^2\sin^2\phi}, \tag{3}$$

where

$$\nabla^2 = \frac{\partial^2}{\partial R^2} + \frac{2}{X}\frac{\partial}{\partial R} + \frac{1}{X^2}\frac{\partial^2}{\partial\phi^2} + \frac{\cot\phi}{X^2}\frac{\partial}{\partial\phi},$$

$$D^2 = \frac{\partial^2}{\partial R^2} + \frac{1}{X^2}\frac{\partial^2}{\partial\phi^2} - \frac{\cot\phi}{X^2}\frac{\partial}{\partial\phi}.$$

Here θ, Ψ and Ω are the dimensionless temperature, stream function and vorticity, respectively; R and X are the dimensionless radial coordinates; ϕ is the latitude angle measured clockwise from the vertically upward position; τ is the dimensionless time; V and U are the dimensionless velocity components in R and ϕ directions, respectively, and Gr and Pr are the Grashof and Prandtl numbers defined as

$$\theta = \frac{T - T_o}{T_i - T_o}, \quad \Psi = Gr^{-1/2}\frac{\psi}{(r_o - r_i)v},$$

$$\Omega = Gr^{-1/2}\frac{\omega(r_o - r_i)^2}{v}, \quad \tau = \frac{tv}{(r_o - r_i)^2}, \quad R = \frac{r - r_i}{r_o - r_i},$$

$$X = \frac{r}{r_o - r_i}, \quad V = Gr^{-1/2}\frac{v(r_o - r_i)}{v} = \frac{1}{X^2\sin\phi}\frac{\partial\Psi}{\partial\phi},$$

$$U = Gr^{-1/2}\frac{u(r_o - r_i)}{v} = -\frac{1}{X\sin\phi}\frac{\partial\Psi}{\partial R},$$

$$Gr = \frac{g\beta(T_i - T_o)(r_o - r_i)^3}{v^2}, \quad Pr = \frac{v}{\alpha}.$$

This scaling is suggested in the literature [19, 20] for Pr of order unity and large Gr. We retain it for $Pr = 0.02$ as well. Also, following de Vahl Davis [20], the energy equation (1) has been multiplied by Pr so that the solution time is almost independent of the Prandtl number. Here, T, ψ, ω, v, u and t are the dimensional counterparts of θ, Ψ, Ω, V, U and τ, respectively, and r is the radial coordinate. Also, T_i, T_o and r_i, r_o are the inner and outer sphere temperatures and radii, respectively, v and α are the kinematic viscosity and thermal diffusivity of the fluid, respectively, g is the acceleration due to gravity, and β is the coefficient of thermal expansion.

Due to axisymmetry (solution independent of the longitude), only half the domain need be considered. The following boundary and initial conditions apply:

$$\Psi = 0, \quad \theta = 1, \quad \Omega = -\frac{1}{X\sin\phi}\frac{\partial^2\Psi}{\partial R^2} \quad \text{at } R = 0,$$

$$\Psi = 0, \quad \theta = 0, \quad \Omega = -\frac{1}{X\sin\phi}\frac{\partial^2\Psi}{\partial R^2} \quad \text{at } R = 1,$$

$$\Psi = 0, \quad \partial\theta/\partial\phi = 0, \quad \Omega = 0 \quad \text{at } \phi = 0, \pi$$

$$\Psi = 0, \quad \theta = 0, \quad \Omega = 0 \quad \text{at } \tau = 0. \tag{4}$$

3. NUMERICAL TECHNIQUE

Following de Vahl Davis [20], we introduce the false transient equations in order to reduce the computer time required for a numerical solution of equations (1)–(4). The changes to the equations are the introduction of false transient factors a_θ, a_Ω and a_Ψ, and the addition of a transient term to equation (2) to turn it into a parabolic equation. Thus equations (1)–(3) are written as

$$\frac{Pr}{a_\theta}\frac{\partial\theta}{\partial\tau} + Pr\,Gr^{1/2}\left(V\frac{\partial\theta}{\partial R} + \frac{U}{X}\frac{\partial\theta}{\partial\phi}\right) = \nabla^2\theta, \tag{5}$$

$$\frac{1}{a_\Psi}\frac{\partial\Psi}{\partial\tau} = D^2\Psi + X\Omega\sin\phi, \tag{6}$$

$$\frac{1}{a_\Omega}\frac{\partial\Omega}{\partial\tau} + Gr^{1/2}\left[V\frac{\partial\Omega}{\partial R} + \frac{U}{X}\frac{\partial\Omega}{\partial\phi} - \frac{\Omega}{X}(V + U\cot\phi)\right]$$
$$= -Gr^{1/2}\left(\sin\phi\frac{\partial\theta}{\partial R} + \frac{\cos\phi}{X}\frac{\partial\theta}{\partial\phi}\right) + \nabla^2\Omega - \frac{\Omega}{X^2\sin^2\phi}. \tag{7}$$

The false transient factors change the time scales of the governing equations, leading to a loss of the true transient solution, but the final steady-state solution, if one exists, is unaffected. Optimum values of these factors, if found, speed up the convergence. Generally, numerical instability arises first in the vorticity equation (7), and a reduction in a_Ω, accompanied by a corresponding increase in a_θ and a_Ψ permits a solution to be obtained for larger parameter values [20]. No attempt was made to optimize the values of false transient factors.

For the finite-difference solution of equations (5), (6), (7) and (4), forward differences are used for the time derivatives and second-order central differences for the space derivatives. The resulting algebraic equations are solved by the alternating direction implicit method, thus solving a set of tridiagonal equations every time. In accordance with de Vahl Davis [20], we found that the cell Reynolds number restriction resulting from the use of second-order central differences for convection terms is not overwhelming due to relatively small velocities in natural convection even at large Grashof numbers. In order to keep the solution numerically stable, the time step $\Delta\tau$ is limited to a value of the order of the square of the smaller of the two mesh sizes ΔR and $\Delta\phi$, with the false transient factors set to unity. In addition to their role in speeding up the convergence, these factors are used to postpone the numerical instability at sufficiently large values of the Grashof number.

It is well known that as the Grashof number increases, the boundary layers on the spheres get thinner and there are large gradients in the ϕ direction

near small values of ϕ. In order to resolve these radial and azimuthal gradients, it is necessary to have a high density of grid points near both spheres and for small values of ϕ. If the grid size is kept uniform, a very large number of grid points would result leading to a solution of a large set of equations. This would require excessive computer time and involve large round-off error. A practical solution is to use a fine mesh size near regions of large gradients, and larger mesh size elsewhere. In order to have a guided, rather than an arbitrary, uneven distribution of grid points, a local one-dimensional grid adaptation, following Nakahashi and Deiwert's method [21], is used. It may be pointed out that a two-dimensional grid adaptation renders the grid non-orthogonal, thus requiring the solution of a complex set of transformed equations owing to the presence of pseudo-diffusive terms. On the other hand, one-dimensional grid adaptation in each direction keeps the grid orthogonal, and, therefore, equations (5), (6), (7) and (4) remain unchanged. However, with an uneven distribution of grid points, the second-order central differences for space derivatives need to be modified, as described by Hornbeck [22].

While numerical experiments were carried out with each of the three variables θ, Ψ and Ω used for adaptation, it was found that, in most cases, adapting the grid in the ϕ direction according to the temperature profile at $R = 1/2$, and in the radial direction according to the vorticity profile at small values of ϕ, that decrease as the Rayleigh number increases, yielded the best results. The number of grid points were taken to be 41 in the radial direction and 46 in the ϕ direction at low Rayleigh numbers, and increased to 81 and 91, respectively, at high Ra. For $Ra < 10^5$, results with a 41×46 grid matched well with those obtained with a 61×61 grid. The final solution of equations (5), (6), (7) and (4) is fed into a very similar code for steady-state equations of motion (without the initial conditions and $\partial/\partial\tau$ terms) to ensure that the solution presented here is the steady-state one. Hardly any iteration was required in this final step.

While the discretization of boundary conditions for Ψ and θ is straightforward, the boundary conditions for Ω in the radial direction are discretized, following Woods [23], as

$$\Omega_b = \frac{-3\Psi_{b+1}}{X_b(\Delta R_b)^2 \sin\phi_b} - \frac{X_{b+1}}{2X_b}\Omega_{b+1}, \qquad (8)$$

where the subscripts 'b' and 'b+1' denote values at a mesh point on the boundary and one mesh length ΔR away from the boundary, respectively. This is a second-order relation, thus matching with the discretization of the governing equations.

4. ACCURACY

A check on the solution is provided by computing the local Nusselt numbers on the inner and outer spheres via the relations [5]

$$Nu_i = -\frac{r_i}{r_o}\left.\frac{\partial\theta}{\partial R}\right|_{R=0}, \quad Nu_o = -\frac{r_o}{r_i}\left.\frac{\partial\theta}{\partial R}\right|_{R=1}.$$

In the steady state, these Nusselt numbers averaged over each of the spheres must be equal, that is,

$$\overline{Nu_i} = \overline{Nu_o} = \frac{k_{eff}}{k},$$

where k_{eff} is the effective conductivity for the spherical annulus. Table 1 lists the values of $\overline{Nu_i}$ and $\overline{Nu_o}$ for a diameter ratio of 2.0 and for various Rayleigh and Prandtl numbers obtained with 41×46, 61×61 and 81×91 grids. Clearly, the difference between $\overline{Nu_i}$ and $\overline{Nu_o}$ is very small for all cases. Table 1 also lists values of $\overline{Nu}$ based upon the empirical equations proposed by Raithby and Hollands [24]

$$\overline{Nu} = \frac{k_{eff}}{k} = 0.74\{Pr/(Pr+0.861)\}^{1/4} \times \left\{\frac{(r_o/r_i-1)^{1/4}(Ra/2)^{1/4}}{(r_o/r_i)[1+(r_o/r_i)^{-7/5}]^{5/4}}\right\}, \qquad (9)$$

and by Scanlan *et al.* [3]

$$\overline{Nu} = \frac{k_{eff}}{k} = 0.228(Ra^*)^{0.226}, \qquad (10)$$

where $Ra^* = Ra$ for $r_o/r_i = 2$. Also tabulated in Table 1 are the percentage differences between our results $(\overline{Nu_i}+\overline{Nu_o})/2$ and those from equations (9) and (10). Since values of $\overline{Nu}$ cannot be less than unity, which is the value for the pure heat conduction solution, we make the $\overline{Nu}$ value unity if it falls below unity as calculated using equation (9) or (10). As expected, all our values are above unity. It is found that equation (9) yields values close to ours for $Pr = 6$, while equation (10) is better at low Rayleigh numbers for $Pr = 0.7$; the maximum difference being about 15%. Scanlan *et al.* [3] note that equation (10) gives an average deviation of 15.6%, and 76% of the experimental data are within $\pm 20\%$ of values predicted by the equation. Comparison with experimental data is thus satisfactory.

5. RESULTS

All the results presented here are for a diameter ratio of 2.0, and $Pr = 0.02$ (liquid metal), 0.7 (air) and 6.0 (water). Results are similar in nature to those for a horizontal, concentric, cylindrical annulus [25], except that steady multi-cellular flow is found for all Prandtl numbers. For validation of the technique, initial solutions were obtained for comparison with previously available results. A comparison was made for $Ra = 14000$ and $Pr = 0.7$ with the results provided by Singh and Chen [7]. The results matched very well. There was excellent agreement between both the isotherms and the streamlines. The maximum value of the dimensionless stream function in our case is 0.2071 while theirs is 0.2076, and the location of this

Table 1. Average Nusselt numbers for $r_o/r_i = 2$

Ra	$\overline{Nu_i}$	$\overline{Nu_o}$	Diff. (%)†	$\overline{Nu}$ from equation (9)	Diff. (%)‡	$\overline{Nu}$ from equation (10)	Diff. (%)§
With 41 × 46 grid; $Pr = 0.7$							
70.0	1.0006	1.0006	0.00	1.0000	0.1	1.0000	0.1
420.0	1.0203	1.0203	0.00	1.0000	2.0	1.0000	2.0
1000.0	1.1006	1.1006	0.00	1.0000	9.1	1.0861	1.3
3000.0	1.4213	1.4212	0.01	1.2610	11.3	1.3924	2.0
6300.0	1.7393	1.7393	0.00	1.5180	12.7	1.6466	5.3
10 500.0	1.9848	1.9847	0.01	1.7248	13.1	1.8481	6.9
14 000.0	2.1331	2.1330	0.00	1.8534	13.1	1.9722	7.5
21 000.0	2.3560	2.3558	0.01	2.0511	12.9	2.1615	8.3
42 000.0	2.7761	2.7763	0.01	2.4392	12.1	2.5281	8.9
91 000.0	3.3110	3.3181	0.21	2.9594	10.7	3.0108	9.2
With 61 × 61 grid; $Pr = 0.7$							
180 000.0	3.8645	3.8702	0.15	3.5096	9.3	3.5126	9.2
250 000.0	4.1637	4.1567	0.17	3.8100	8.4	3.7833	9.1
With 41 × 46 grid; $Pr = 6$							
600.0	1.0405	1.0405	0.00	1.0000	3.9	1.0000	3.9
1500.0	1.1958	1.1958	0.00	1.2531	4.8	1.1905	0.4
3000.0	1.4489	1.4489	0.00	1.4902	2.8	1.3924	3.9
7350.0	1.8790	1.8790	0.00	1.8643	0.8	1.7049	9.3
18 000.0	2.3633	2.3632	0.00	2.3323	1.3	2.0875	11.7
45 000.0	2.9237	2.9259	0.08	2.9327	0.3	2.5678	12.2
90 000.0	3.4237	3.4248	0.03	3.4877	1.8	3.0034	12.3
180 000.0	4.0256	4.0067	0.47	4.1476	3.3	3.5127	12.5
360 000.0	4.7474	4.7077	0.84	4.9323	4.3	4.1084	13.1
With 81 × 91 grid; $Pr = 6$							
180 000.0	4.0239	4.0223	0.04	4.1474	3.1	3.5126	12.7
360 000.0	4.7471	4.7510	0.08	4.9321	3.9	4.1083	13.5
660 000.0	5.4900	5.5023	0.22	5.7391	4.4	4.7114	14.3
1 000 000.0	6.0661	6.0829	0.28	6.3673	4.8	5.1753	14.8
With 41 × 46 grid; $Pr = 0.02$							
400.0	1.0127	1.0127	0.00	1.0000	1.3	1.0000	1.3
1000.0	1.0486	1.0485	0.01	1.0000	4.6	1.0863	3.6
1500.0	1.0817	1.0816	0.01	1.0000	7.5	1.1905	10.1
1800.0	1.1020	1.1019	0.01	1.0000	9.3	1.2406	12.6

† Difference between the present $\overline{Nu_i}$ and $\overline{Nu_o}$.
‡ Difference between the present $\overline{Nu}$ and that from equation (9).
§ Difference between the present $\overline{Nu}$ and that from equation (10).

maximum coincides exactly. Moreover, while our $\overline{Nu} = 2.1331$, Singh and Chen [7] found a value of 2.1439.

A solution similar to the one presented by Mack and Hardee [5] for $Ra = 1000$ and $Pr = 0.7$ was also obtained. Based upon earlier validation of our method, we find that the temperature profiles given by Mack and Hardee for $\phi \leqslant 40°$ are in error, resulting from an inadequate number of terms summed in their series solution. For this case, our $\overline{Nu} = 1.1006$, while Mack and Hardee [5] report a value of 1.12 and Singh and Chen [7] report values of 1.1010 and 1.1007 obtained with three and five terms, respectively, in their series solution.

The flow and heat transfer results can be divided into several regimes depending upon the Rayleigh number. Up to a $Ra \sim O(10^2)$, pure conduction dominates the flow; the velocities being too small to affect the temperature distribution. The center of rotation (location of Ψ_{max}) is near 90°. The flow in the top and bottom portions of the annulus is symmetrical about the 90° position. As the Rayleigh number increases, the center of rotation moves upward. The flow remains in essentially the same pattern but becomes strong enough to influence the temperature field. The isotherms form eccentric circles near a Ra of 10^3. With a further increase in Ra, the temperature distribution gets distorted, resulting in higher overall heat transfer.

At a Rayleigh number of about 7350, radial temperature inversion sets in, indicating the separation of inner- and outer-sphere thermal boundary layers. Thus, the fluid near the cool outer-sphere is warmer than that closer to the hot inner-sphere. This phenomenon has also been observed in natural convection between concentric cylinders [25] and in a vertical slot [26]. Heat is convected from the lower portion of the inner-sphere to the top of the outer-sphere. As shown in Fig. 1, vorticity in the central core is almost constant near and above this Ra, indicating a region approaching solid-body rotation, and similar to flow in a vertical slot [27]. Figures 1 and 2 show the Ω values normalized by $|\Omega|_{max}$ at various latitude angles. At lower Rayleigh numbers, vorticity is well distributed within the annulus. At much higher Rayleigh

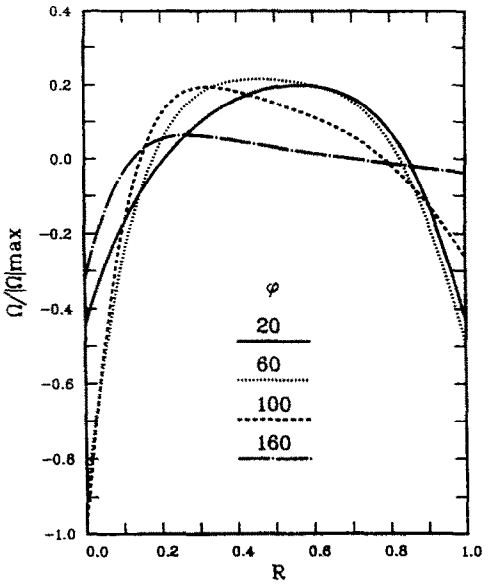

FIG. 1. Vorticity distribution for $Ra = 7350$ and $Pr = 6$ at various angular positions. $|\Omega|_{max} = 3.156$.

numbers, vorticity approaches zero in most of the central portion of the annulus, as shown in Fig. 2 for $Ra = 6.6 \times 10^5$ and $Pr = 6$. This implies a stationary core region, and is similar to the natural convection flow in a vertical slot [28].

Figure 3 shows the isotherms and streamlines for $Ra = 9 \times 10^4$ and $Pr = 6$. The isotherms in this and later figures have been drawn at intervals of 0.1. Similarly, the streamlines in all the results presented here have been drawn at intervals of $\Psi_{max}/10$. The sign $\times$ indicates the location of Ψ_{max}, also known as the center of rotation for the fluid in the half annulus. As

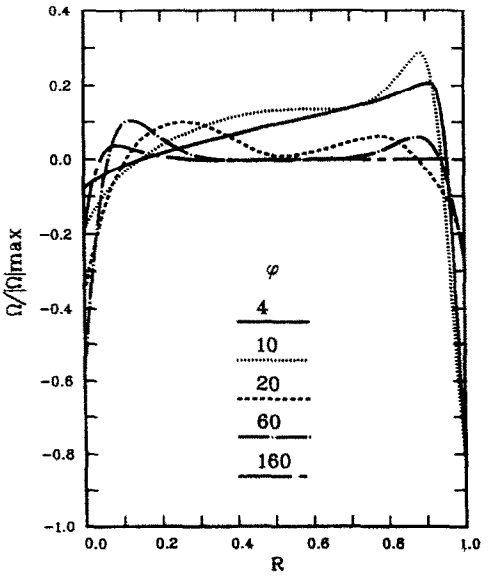

FIG. 2. Vorticity distribution for $Ra = 6.6 \times 10^5$ and $Pr = 6$ at various angular positions. $|\Omega|_{max} = 15.52$.

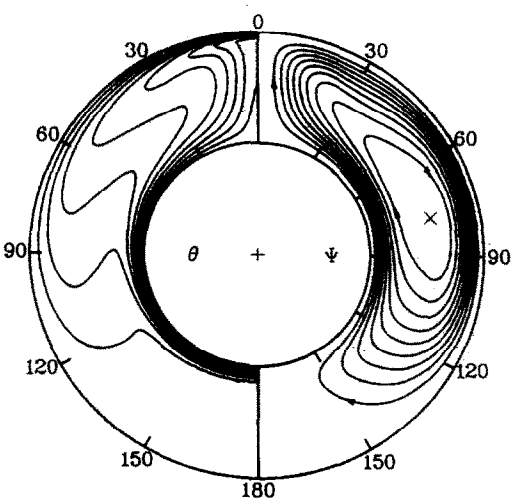

FIG. 3. Isotherms and streamlines for $Ra = 9 \times 10^4$ and $Pr = 6$. $\Psi_{max} = 0.046$.

is clear from Fig. 3, the almost stagnant region in the bottom of the annulus is quite large, and it increases with Ra. We may note that the results for this case given by Singh and Chen [7] are in error. As admitted by them, their solution for this case should have included more terms in the series solution. A major short-coming of their numerical technique is that as the Grashof number increases, the number of terms required for accurate solution increases, resulting in a rapid increase in the amount of computation. For this reason, they could not get accurate results for moderate Gr of 15000, and no convergence for $Gr > 20000$.

As the Rayleigh number increases further, the most common flow pattern, the 'crescent eddy' type, shown by the streamlines in Fig. 3, changes to a 'kidney-shaped eddy' type of flow, as shown in Fig. 4 for

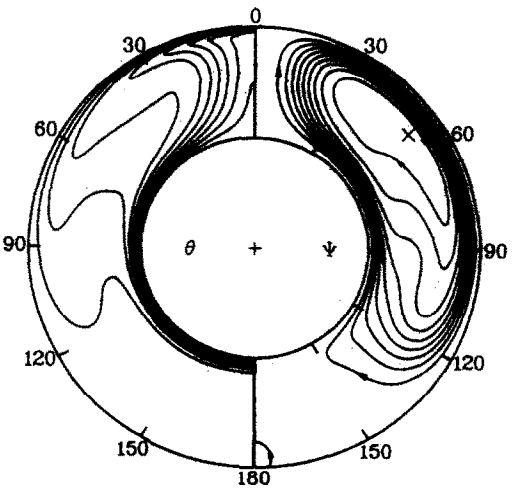

FIG. 4. Isotherms and streamlines for $Ra = 2.5 \times 10^5$ and $Pr = 0.7$. $\Psi_{max} = 0.105$.

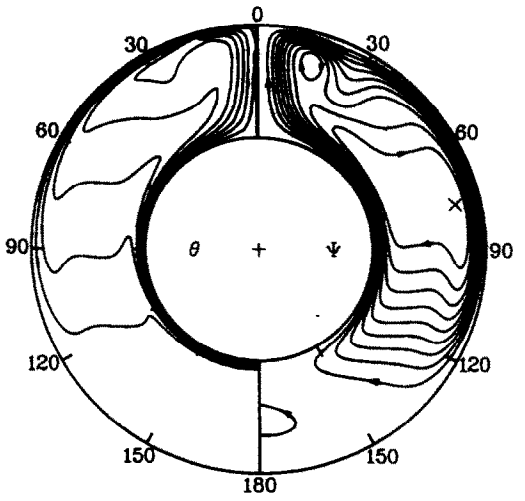

FIG. 5. Isotherms and streamlines for $Ra = 10^6$ and $Pr = 6$. $\Psi_{max} = 0.024$.

$Ra = 2.5 \times 10^5$ and $Pr = 0.7$, and in Fig. 5 for $Ra = 10^6$ and $Pr = 6$. Since the kidney eddy type differs only qualitatively from the crescent eddy type in the shape of streamlines in the low-speed central eddy region, the heat transfer characteristics of the two types of flow are similar. Streamlines in Fig. 5 compare very well with the flow pattern found experimentally in the Fig. 8 of Yin *et al.* [4], while those in Fig. 4 are similar to the experimental flow pattern in the Fig. 5 of Bishop *et al.* [2]. Moreover, both Figs. 4 and 5 show a small anti-clockwise rotating secondary cell in the bottom of the annulus, while the primary central eddy is clockwise. For both $Pr = 0.7$ and 6.0, this secondary cell appears at $Ra \approx 1.6 \times 10^5$ near the bottom of the outer-sphere. As Ra increases, the secondary cell grows and moves towards the inner-sphere; Fig. 5 shows its location between the two spheres at $\phi \approx 180°$. Of course, the secondary cell represents small negative values of the stream function. We may note that in experiments with air in a spherical annulus of diameter ratio 1.19, Bishop *et al.* [2] found two secondary cells having a sense of rotation opposite to that of the primary central eddy at high Rayleigh numbers. One of these cells was found near the top of the inner-sphere, and the other at the bottom of the outer-sphere. Ingham [9], however, did not find any secondary cell numerically for the same parameters. For the much higher diameter ratio of 2, we find only one secondary cell at the bottom of the annulus for both air and water at Rayleigh numbers of order 10^5.

Figure 6 shows the temperature profiles at various angular positions for $Ra = 10^6$ and $Pr = 6$. The large temperature gradients in the radial direction near both the spheres, and in the latitude direction for small ϕ values are clearly evident. This calls for high grid resolution, pointing to the usefulness of grid adaptation, near both spheres and for $\phi \leqslant 30°$ at high Rayleigh numbers. Also worthy of note in Fig. 6 are the temperature inversions in the core of the annulus.

For liquid metals, the multi-cellular flow really comes to life, as shown in Figs. 7–9. Figure 7 shows the isotherms and streamlines for $Gr = 20\,000$ and $Pr = 0.02$. It may be noted that results given by Singh and Chen [7] for this case are wrong. As reported by them, they did not get convergence for these parameter values. Besides, they did not find the small secondary cell at the top of the annulus near the outer sphere. This cell has an anti-clockwise rotation, while the main eddy is clockwise. As the Grashof number increases, more cells are formed, as shown in Fig. 8 for $Gr = 50\,000$ and in Fig. 9 for $Gr = 90\,000$, both for $Pr = 0.02$. In both Figs. 8 and 9, the clockwise cell

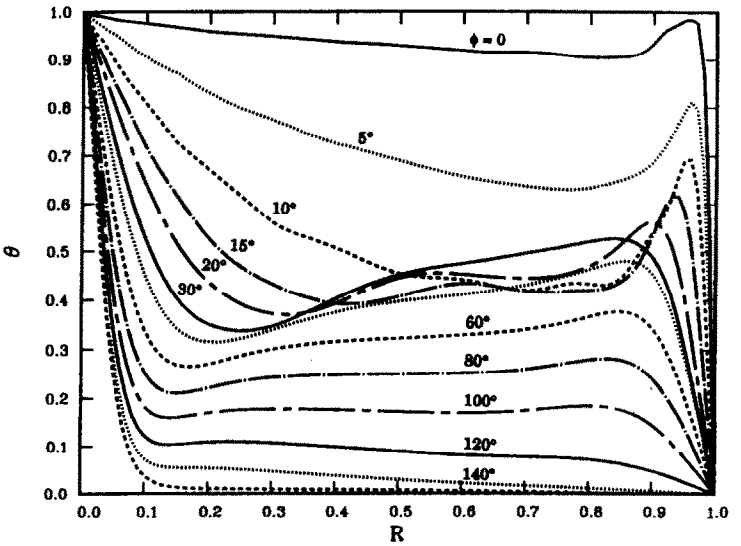

FIG. 6. Temperature profiles for $Ra = 10^6$ and $Pr = 6$ at various angular positions. (——) $\phi = 0, 30, 120°$; (···) $\phi = 5, 40, 140°$; (- - -) $\phi = 10, 60, 180°$; (—·—) $\phi = 15, 80°$; (—- -—) $\phi = 20, 100°$.

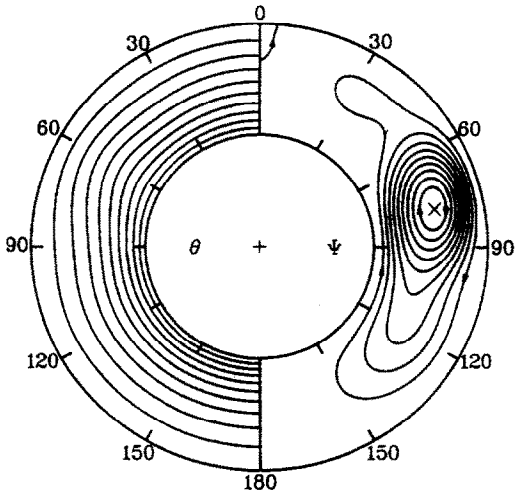

FIG. 7. Isotherms and streamlines for $Gr = 20000$ and $Pr = 0.02$. $\Psi_{max} = 0.459$.

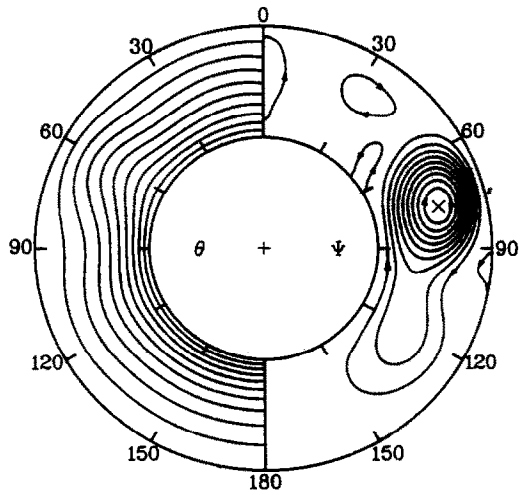

FIG. 8. Isotherms and streamlines for $Gr = 50000$ and $Pr = 0.02$. $\Psi_{max} = 0.579$.

at about 30° position corresponds to $\Psi/\Psi_{max} = 0.1$. The anti-clockwise cells are weaker than the main eddy. Looking at Figs. 7–9, one notices that the small anti-clockwise cell at the top of the annulus in Fig. 7 grows in Fig. 8 and breaks up into two counter-rotating cells in Fig. 9. With so many cells appearing in the flow domain, much smaller steps in Gr have to be taken to ensure convergence of the solution near a Grashof number of 90000. The isotherms are almost concentric circles at $Gr = 20000$ (Fig. 7) but get distorted (differently than those for $Pr = 0.7$ and 6.0) as Gr increases (Figs. 8 and 9). Since the bulk of the motion is confined around $\phi = 90°$, more distortion of the isotherms takes place in this region.

Figure 10 provides the variation of maximum values of stream function, vorticity, and speed in the annulus with the Grashof number. It may be noted that the maximum speed, S_{max}, scales with the Grashof

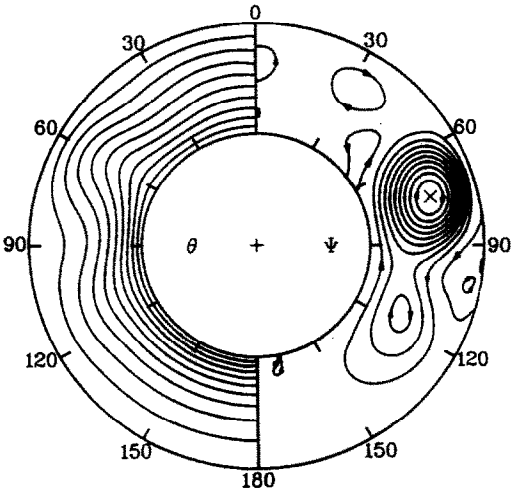

FIG. 9. Isotherms and streamlines for $Gr = 90000$ and $Pr = 0.02$. $\Psi_{max} = 0.649$.

number rather than the Rayleigh number. In fact, the effect of Pr on S_{max} and $|\Omega|_{max}$ is very small for all Grashof numbers. This figure also shows that, for large Grashof numbers, the maximum value of stream function within the spherical annulus decreases as the Prandtl number increases.

The local Nusselt numbers of the inner- and outer-spheres, Nu_i and Nu_o, at various latitude angles are shown in Figs. 11 and 12, respectively, as a function of the Rayleigh number for $Pr = 0.7$ and 6.0. The Nusselt number approaches unity in the conduction regime for Ra below 100. On both the spheres, some local values are larger than unity while others are less than unity at the same Rayleigh number. The dashed curves in Figs. 11 and 12 represent the variation of the average Nusselt number with the Rayleigh number; the lower curve being for $Pr = 0.7$. A small effect of the Prandtl number is also visible in these figures. The Nusselt number is generally smaller and more uniform at lower Prandtl number. Results for $Pr = 0.02$ are not given since Nusselt number values in this case are close to unity for the range of Rayleigh numbers investigated. The maximum Rayleigh number for $Pr = 0.02$ was 1800, and the average Nusselt number was 1.1.

Clearly, the largest temperature gradient and heat flux occur at the stagnation point, while the largest boundary layer thickness and smallest temperature gradient occur at the separation point. Thus, for the inner-sphere, the local heat flux at the bottom is the largest while that at the top is small. For the outer-sphere, the stagnation point is at the top along with the high heat flux, while the separation point is at the bottom resulting in the low heat flux there. The buoyant plume above the inner-sphere impinges upon the outer-sphere at the top, creating the thinnest boundary layer and the highest heat flux for the system. This warm fluid then moves down the boundary layer adjacent to the outer-sphere. For this reason,

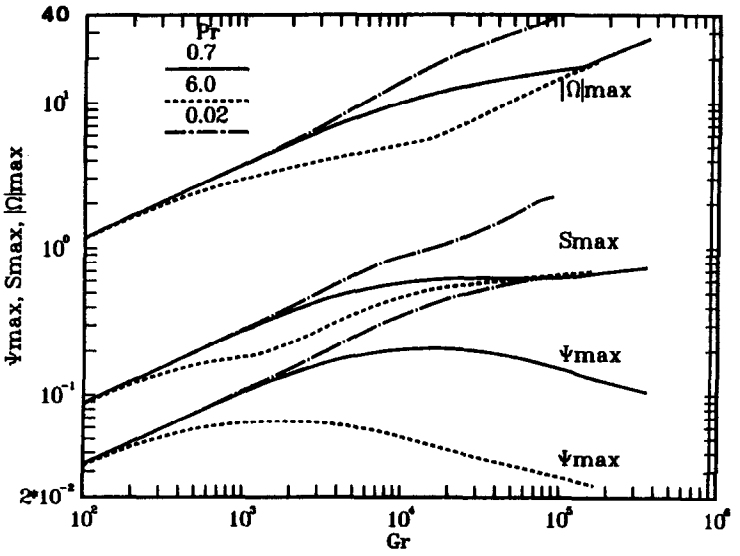

FIG. 10. Maximum values of stream function, speed, and vorticity as a function of Gr for three Pr values.

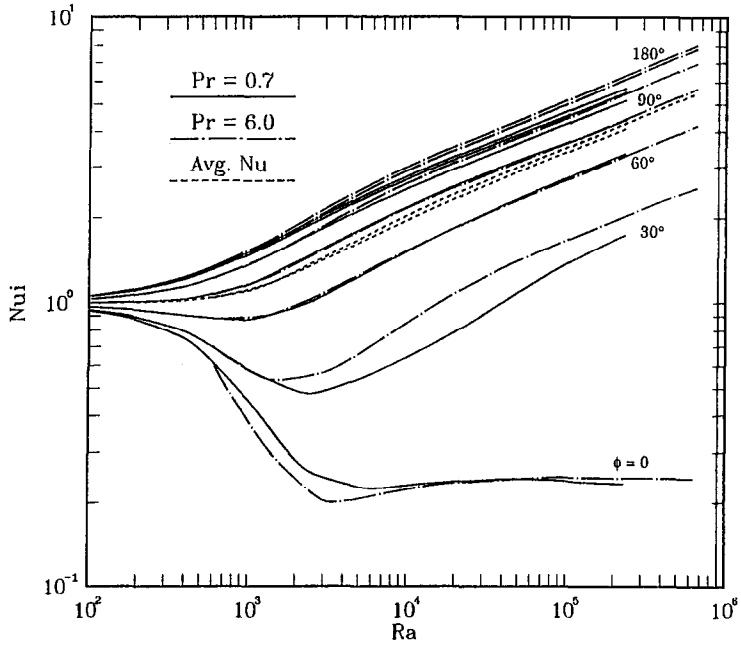

FIG. 11. Local Nusselt number on the inner-sphere as a function of Ra at 30° intervals in ϕ.

higher resolution is required for $\phi \leqslant 30°$ at Rayleigh numbers greater than about 10^5. The presence of boundary layers on both walls and the large gradients near the top suggests that the mesh points be closely spaced for $\phi \leqslant 30°$ in the ϕ direction, and near both the spheres ($R = 0$ and 1) in the radial direction. Grid adaptation is specially useful for the large Rayleigh numbers.

6. CONCLUSIONS

An efficient numerical technique for the study of natural convection flow in a concentric spherical annulus with isothermal walls has been described. Results are presented for a diameter ratio of 2 and three Prandtl numbers, 0.02, 0.7 and 6. The Rayleigh number based on the gap width varies from about 10^2 to 10^6. Accurate results for higher Rayleigh numbers can be easily computed. The break-up into multicellular flow is found at high Rayleigh numbers for air and water, and at significantly low Rayleigh numbers for liquid metals. Results for the vorticity distribution within the spherical annulus are also provided. Unlike previous methods, the present technique is quite efficient and robust in yielding accurate results for high Rayleigh numbers.

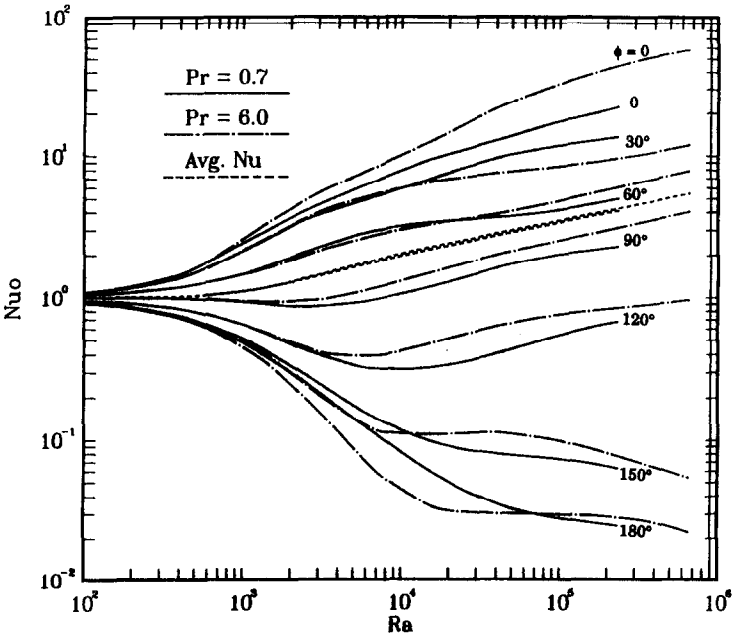

FIG. 12. Local Nusselt number on the outer-sphere as a function of Ra at 30° intervals in ϕ.

Acknowledgements—Support from the Pittsburgh Supercomputing Center for use of its CRAY Y-MP/832 is gratefully acknowledged. Also acknowledged are the referees for their useful comments.

REFERENCES

1. E. H. Bishop, R. S. Kolflat, L. R. Mack and J. A. Scanlan, Convective heat transfer between concentric spheres, *Proc. 1964 Heat Transfer Fluid Mech. Inst.* (Edited by W. H. Giedt and S. Levy), pp. 69–80. Stanford University Press, Berkeley, California (1964).
2. E. H. Bishop, L. R. Mack and J. A. Scanlan, Heat transfer by natural convection between concentric spheres, *Int. J. Heat Mass Transfer* **9**, 649–662 (1966).
3. J. A. Scanlan, E. H. Bishop and R. E. Powe, Natural convection heat transfer between concentric spheres, *Int. J. Heat Mass Transfer* **13**, 1857–1872 (1970).
4. S. H. Yin, R. E. Powe, J. A. Scanlan and E. H. Bishop, Natural convection flow patterns in spherical annuli, *Int. J. Heat Mass Transfer* **16**, 1785–1795 (1973).
5. L. R. Mack and H. C. Hardee, Natural convection between concentric spheres at low Rayleigh numbers, *Int. J. Heat Mass Transfer* **11**, 387–396 (1968).
6. R. J. Brown, Natural convection heat transfer between concentric spheres, Ph.D. dissertation, University of Texas, Austin (1967).
7. S. N. Singh and J. Chen, Numerical solution for free convection between concentric spheres at moderate Grashof numbers, *Numer. Heat Transfer* **3**, 441–459 (1980).
8. J. P. Caltagirone, M. Combarnous and A. Mojtabi, Natural convection between two concentric spheres: transition toward a multicellular flow, *Numer. Heat Transfer* **3**, 107–114 (1980).
9. D. B. Ingham, Heat transfer by natural convection between spheres and cylinders, *Numer. Heat Transfer* **4**, 53–67 (1981).
10. T. Fujii, T. Honda and M. Fujii, A numerical analysis of laminar free convection around an isothermal sphere: finite-difference solution of the full Navier–Stokes and energy equations between concentric spheres, *Numer. Heat Transfer* **7**, 103–111 (1984).
11. S. N. Singh and J. M. Elliott, Natural convection between concentric spheres in a slightly-thermally stratified medium, *Int. J. Heat Mass Transfer* **24**, 395–406 (1981).
12. A. Mojtabi and J. P. Caltagirone, Natural convection between two concentric spheres for high Prandtl number, *Proc. 7th Int. Heat Transfer Conf.*, Munich, Vol. 2, pp. 245–249. Hemisphere, New York (1982).
13. J. Nelsen, R. Douglass and D. Alexander, Natural convection in a spherical annulus filled with heat generating fluid, *Proc. 7th Int. Heat Transfer Conf.*, Munich, Vol. 2, pp. 171–176. Hemisphere, New York (1982).
14. J. M. Nelsen and R. W. Douglass, On partial spectral expansions with natural convection in spherical annulus enclosures as an example, *Numer. Heat Transfer* **6**, 67–84 (1983).
15. J. M. Nelsen and R. W. Douglass, Non-uniform energy generation effects on natural convection in a spherical annulus enclosure, *Int. J. Heat Mass Transfer* **27**, 1925–1928 (1984).
16. J. L. Wright and R. W. Douglass, Natural convection in narrow-gap, spherical annuli, *Int. J. Heat Mass Transfer* **29**, 725–739 (1986).
17. D. R. Gardner, R. W. Douglass and S. A. Trogdon, Linear stability of natural convection in spherical annuli, *J. Fluid Mech.* **221**, 105–129 (1990).
18. P. J. Burns and C. L. Tien, Natural convection in porous media bounded by concentric spheres and horizontal cylinders, *Int. J. Heat Mass Transfer* **22**, 929–939 (1979).
19. S. Ostrach, Natural convection in enclosures, *J. Heat Transfer* **110**, 1175–1190 (1988).
20. G. de Vahl Davis, Finite difference methods for natural and mixed convection in enclosures, *Proc. 8th Int. Heat Transfer Conf.*, San Francisco, Vol. 1, pp. 101–109. Hemisphere, New York (1986).
21. K. Nakahashi and G. S. Deiwert, Self-adaptive-grid method with application to airfoil flow, *AIAA J.* **25**, 513–520 (1987).
22. R. W. Hornbeck, Numerical marching techniques in fluid flows with heat transfer, NASA SP-297 (1973).
23. L. C. Woods, A note on the numerical solution of fourth order differential equations, *Aero. Quart.* **5**, 176–184 (1954).

24. G. D. Raithby and K. G. T. Hollands, A general method of obtaining approximate solutions to laminar and turbulent free convection problems, *Adv. Heat Transfer* **11**, 265–315 (1975).
25. T. H. Kuehn and R. J. Goldstein, An experimental and theoretical study of natural convection in the annulus between horizontal concentric cylinders, *J. Fluid Mech.* **74**, 695–719 (1976).
26. R. K. MacGregor and A. F. Emery, Free convection through vertical plane layers—moderate and high Prandtl number fluids, ASME Paper No. 68-HT-4 (1968).
27. G. K. Batchelor, Heat transfer by free convection across a closed cavity between vertical boundaries at different temperatures, *Quart. Appl. Math.* **12**, 209–233 (1954).
28. A. Rubel and F. Landis, Numerical study of natural convection in a vertical rectangular enclosure, *Physics Fluids Suppl.* **12**(II), 208–213 (1969).

CONVECTION NATURELLE ENTRE DES SPHERES CONCENTRIQUES

Résumé—On obtient une solution par différences finies de l'écoulement convectif dans un espace entre sphères concentriques avec parois isothermes. La formulation fonction de courant–vorticité des équations du mouvement est utilisée pour traiter la solution finale de l'état permanent. La méthode implicite des directions alternées est utilisée pour la résolution des équations discrètes avec une adaptation de grille monodimensionnelle locale pour les sauts de gradient dans quelques régions de l'écoulement aux grands nombres de Rayleigh. On trouve la division en écoulements multicellulaires aux grands nombres de Rayleigh pour l'air et l'eau et à faibles nombres de Rayleigh pour les métaux liquides. On obtient un excellent accord entre les données expérimentales antérieures et les calculs.

NATÜRLICHE KONVEKTION ZWISCHEN KONZENTRISCHEN KUGELN

Zusammenfassung—Mit Hilfe eines Finite-Differenzen-Verfahrens wird die stationäre natürliche Konvektion in einem Ringspalt zwischen zwei konzentrischen Kugeln mit isothermen Oberflächen berechnet. Für die Impulsgleichungen der nichtstationären achsensymmetrischen Strömung wird die Stromfunktions-Wirbeltransportformulierung verwendet; das Interesse liegt jedoch bei der sich am Ende einstellenden stationären Lösung. Für die zeitlichen Ableitungen werden Vorwärtsdifferenzen verwendet, für die räumlichen Ableitungen zentrale Differenzen zweiter Ordnung. Für die Lösung der diskretisierten Gleichungen wird die implizite Methode der alternierenden Richtungen benutzt. Örtliche eindimensionale Gitteranpassung wird herangezogen, um die übermäßig steilen Gradienten in einigen Bereichen der Strömung bei großen Rayleigh-Zahlen aufzulösen. Bei hohen Rayleigh-Zahlen ergibt sich im Fall von Luft und Wasser ein Aufbrechen in eine multizellulare Strömung, bei flüssigen Metallen ist dies bei recht kleinen Rayleigh-Zahlen der Fall. Die Übereinstimmung mit früheren experimentellen und numerischen Ergebnissen ist exzellent.

ЕСТЕСТВЕННАЯ КОНВЕКЦИЯ МЕЖДУ КОНЦЕНТРИЧЕСКИМИ СФЕРАМИ

Аннотация—Конечно-разностным методом получено решение задачи стационарного естественно-конвективного течения в кольцевом канале с изотермическим стенками, образованном концентрическими сферами. Уравнения движения для нестационарного осесимметрижного течения даны в формулировке функция тока–завихренность, причем основной интерес представляет конечное стационарное решение. Для временных производных используются правые разности, а для пространственных–центральные разности второго порядка. Конечно-разностные уравнения решаются неявным методом переменных направлений. Для анализа больших градиентов в некоторых областях течения при высоких числах Рэлея применяется локальная адаптация одномерной сетки. Обнаружено разделение на многоячеистое течение при высоких числах Рэлея в случае воздуха и воды и при существенно низких числах Рэлея в случае жидких металлов. Получено очень хорошее согласие с предыдущими экспериментальными и численными данными.